Molecular switch between structural compaction and thermodynamic stability by interface Xxx-Pro in transmembrane β-barrels

Bharat Ramasubramanian Iyer, Swadha Gupta,[a] Henna Noordeen,[a] Roshika Ravi,[b] Meera Daulatrao Pawar,[b] Anjana George,[b] and Radhakrishnan Mahalakshmi*

Molecular Biophysics Laboratory, Department of Biological Sciences, Indian Institute of Science Education and Research, Bhopal, India.

[a,b]Equal contribution.

*Corresponding author. E-mail: maha@iiserb.ac.in.

SUPPORTING MATERIAL

SI TABLE

Table S1. Thermodynamic parameters for the PagP-X^{160}P^{161} series from equilibrium chemical denaturation.

PagP Variants [@]	First transition [#] $\Delta G^0_{F,1}$ (kcal mol^{-1})	Second transition [#] $\Delta G^0_{F,2}$ (kcal mol^{-1})	Total ΔG^0_F (kcal mol^{-1})	$\Delta\Delta G^0_{XP\text{-}QP}$ (kcal mol^{-1})	$\Delta\Delta G^0_{XP\text{-}QF}$ [$] (kcal mol^{-1})
A^{160}P^{161}	-6.04 ± 0.42	-9.97 ± 0.55	-16.01 ± 0.69	-11.23 ± 0.69	-4.21 ± 1.09
C^{160}P^{161}	-7.82 ± 0.28	-11.78 ± 0.33	-19.60 ± 0.43	-14.82 ± 0.44	-7.80 ± 0.94
D^{160}P^{161}	-4.55 ± 0.60	-9.64 ± 0.25	-14.19 ± 0.65	-9.41 ± 0.65	-2.39 ± 1.06
E^{160}P^{161}	-4.52 ± 0.07	--	-4.52 ± 0.07	0.26 ± 0.10	7.28 ± 0.84
F^{160}P^{161}	-4.86 ± 0.70	-10.89 ± 0.38	-15.75 ± 0.80	-10.97 ± 0.80	-3.95 ± 1.16
G^{160}P^{161}	-4.59 ± 0.07	--	-4.59 ± 0.07	0.19 ± 0.10	7.21 ± 0.84
H^{160}P^{161}	-5.53 ± 1.20	-9.67 ± 1.99	-15.20 ± 2.33	-10.42 ± 2.33	-3.40 ± 2.48
I^{160}P^{161}	-5.02 ± 1.09	-9.25 ± 1.90	-14.27 ± 2.19	-9.49 ± 2.19	-2.47 ± 2.35
K^{160}P^{161}	-5.18 ± 0.43	-10.65 ± 0.54	-15.83 ± 0.69	-11.05 ± 0.69	-4.03 ± 1.09
L^{160}P^{161}	-6.25 ± 0.69	-9.88 ± 0.34	-16.13 ± 0.77	-11.35 ± 0.77	-4.33 ± 1.14
M^{160}P^{161}	-4.10 ± 1.06	-9.87 ± 1.95	-13.97 ± 2.22	-9.19 ± 2.22	-2.17 ± 2.37
N^{160}P^{161}	-4.57 ± 0.07	--	-4.57 ± 0.07	0.21 ± 0.10	7.23 ± 0.84
P^{160}P^{161}	-4.50 ± 0.07	--	-4.50 ± 0.07	0.28 ± 0.10	7.30 ± 0.84
Q^{160}P^{161}	-4.78 ± 0.07	--	-4.78 ± 0.07	0	7.02 ± 0.84
R^{160}P^{161}	-5.75 ± 0.34	-9.74 ± 0.45	-15.49 ± 0.56	-10.71 ± 0.56	-3.69 ± 1.01
S^{160}P^{161}	-6.53 ± 0.10	--	-6.53 ± 0.10	-1.75 ± 0.12	5.27 ± 0.85
T^{160}P^{161}	-4.98 ± 0.08	--	-4.98 ± 0.08	-0.20 ± 0.11	6.82 ± 0.84
V^{160}P^{161}	-4.35 ± 0.68	-9.30 ± 0.37	-13.65 ± 0.77	-8.87 ± 0.77	-1.85 ± 1.14
W^{160}P^{161}	-4.35 ± 0.41	-10.11 ± 0.20	-14.46 ± 0.46	-9.68 ± 0.47	-2.66 ± 0.96
Y^{160}P^{161}	-6.18 ± 0.42	-9.42 ± 0.28	-15.60 ± 0.51	-10.82 ± 0.51	-3.80 ± 0.98

[@] Mutants are labeled based on the interface residue mutations, using the single letter code of the amino acid followed by the residue number (in superscript) wherein the substitution has been carried out.

[#] Mutants displaying two-state behavior were fitted using a shared *m* value of 1.69 ± 0.03 kcal mol^{-1} M^{-1}. For the analysis of the three-state mutants, we used two shared *m* values of m_1 = 2.54 ± 0.68 kcal mol^{-1} M^{-1} and m_2 = 2.88 ± 0.50 kcal mol^{-1} M^{-1}.

[$] PagP-QF is the wild type PagP.

Table S2. Thermodynamic parameters for the PagP-X^{160}P^{161} mutant series derived from two-state folding analysis.

PagP Variants[@]	ΔG^0_F (kcal mol^{-1})[#]	C_m (M)	$\Delta\Delta G^0_{XP\text{-}QF}$ (kcal mol^{-1})	ΔG_{int} (kcal mol^{-1})
A^{160}P^{161}	-4.66 ± 0.04	2.76 ± 0.02	7.14 ± 0.84	0.32 ± 1.02
C^{160}P^{161}	-5.11 ± 0.06	3.02 ± 0.04	6.69 ± 0.84	-9.06 ± 0.85
D^{160}P^{161}	-4.86 ± 0.04	2.87 ± 0.03	6.94 ± 0.84	-7.16 ± 0.86
E^{160}P^{161}	-4.52 ± 0.07	2.68 ± 0.02	7.28 ± 0.84	-1.36 ± 1.06
F^{160}P^{161}	-4.66 ± 0.07	2.76 ± 0.04	7.14 ± 0.84	12.07 ± 0.85
G^{160}P^{161}	-4.59 ± 0.07	2.72 ± 0.02	7.21 ± 0.84	1.14 ± 0.99
H^{160}P^{161}	-4.73 ± 0.05	2.80 ± 0.03	7.07 ± 0.84	-2.01 ± 1.02
I^{160}P^{161}	-4.43 ± 0.05	2.62 ± 0.03	7.37 ± 0.84	5.36 ± 0.85
K^{160}P^{161}	-4.52 ± 0.05	2.67 ± 0.03	7.28 ± 0.84	-4.39 ± 0.87
L^{160}P^{161}	-4.96 ± 0.05	2.94 ± 0.03	6.84 ± 0.84	3.14 ± 0.85
M^{160}P^{161}	-4.08 ± 0.05	2.42 ± 0.03	7.72 ± 0.84	3.14 ± 0.85
N^{160}P^{161}	-4.57 ± 0.07	2.70 ± 0.02	7.23 ± 0.84	-6.21 ± 0.86
P^{160}P^{161}	-4.50 ± 0.07	2.67 ± 0.02	7.30 ± 0.84	-3.21 ± 0.92
Q^{160}P^{161}	-4.78 ± 0.07	2.83 ± 0.02	7.02 ± 0.84	--
R^{160}P^{161}	-4.65 ± 0.04	2.75 ± 0.02	7.15 ± 0.84	-2.18 ± 0.96
S^{160}P^{161}	-6.53 ± 0.10	3.87 ± 0.02	5.27 ± 0.85	1.36 ± 1.09
T^{160}P^{161}	-4.98 ± 0.08	2.95 ± 0.02	6.82 ± 0.84	0.93 ± 1.03
V^{160}P^{161}	-4.43 ± 0.04	2.62 ± 0.02	7.37 ± 0.84	3.24 ± 0.84
W^{160}P^{161}	-4.56 ± 0.07	2.70 ± 0.04	7.24 ± 0.84	0.37 ± 0.85
Y^{160}P^{161}	-4.90 ± 0.06	2.90 ± 0.04	6.90 ± 0.84	-11.92 ± 0.85

[@] Mutants are labeled based on the interface residue mutations using the single letter code of the amino acid followed by the residue number (in superscript) at which the substitution has been carried out.

[#] All the mutants, regardless of whether they display two-state or three-state folding behavior, were fit using a global *m* value of 1.69 ± 0.03 kcal mol^{-1} M^{-1}.

SI FIGURES

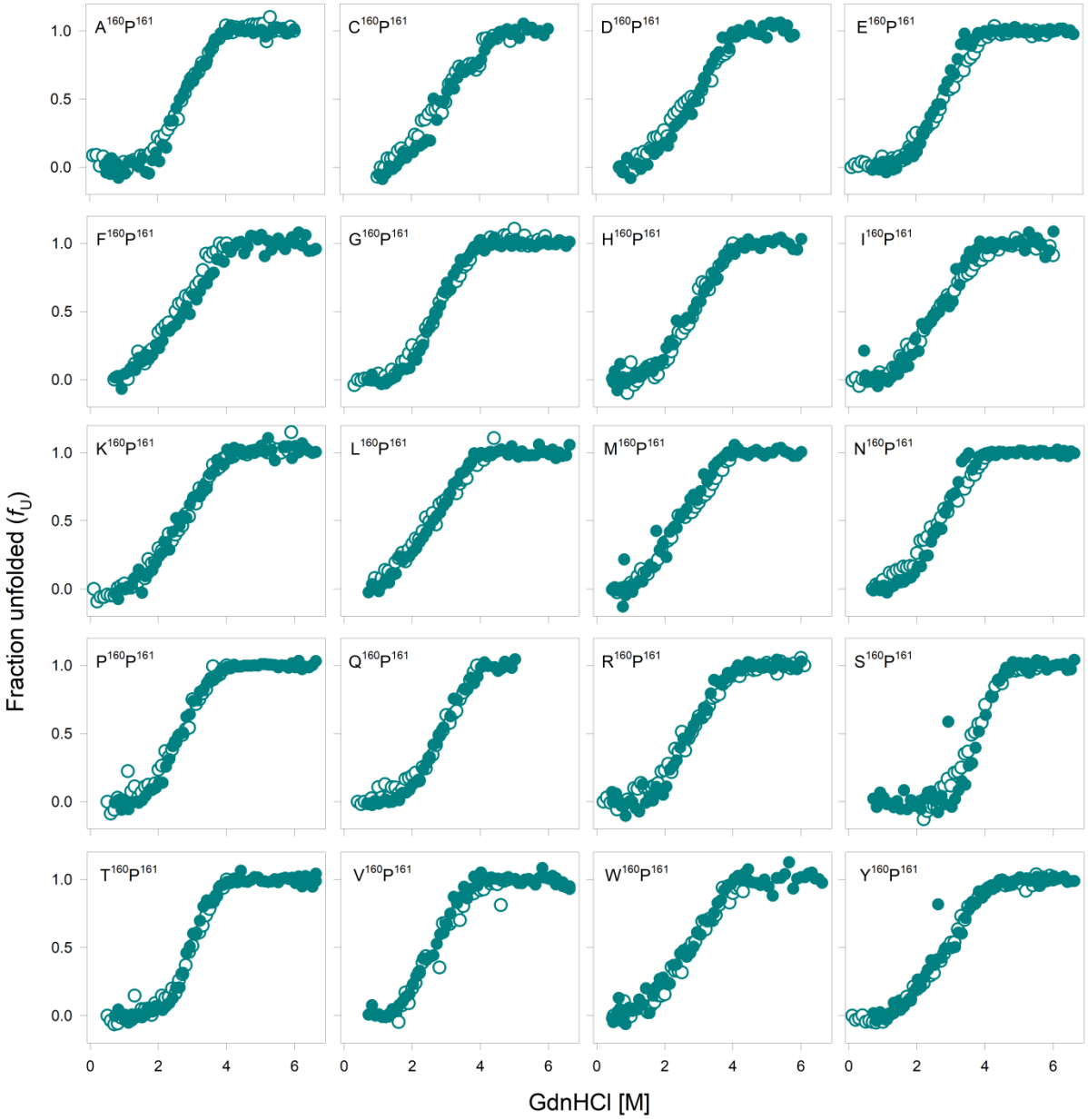

Figure S1. Equilibrium titrations of PagP-X^{160}P^{161} library demonstrate path independence. Representative unfolding (open symbols) and folding (filled symbols) profiles derived using the measured change in fluorescence emission intensity of the 12 intrinsic tryptophans of PagP, at the λ_{em} of 344 nm, which corresponds to the $\lambda_{em\text{-}max}$ of the folded protein. It is to be noted here that PagP-W^{160}P^{161} has an additional tryptophan. We normalized the fluorescence emission intensity between 0 and 1, with 1 representing the fluorescence intensity of the fully unfolded state. Thereafter, we computed the unfolded fraction (f_U) and plotted it against the denaturant concentration. Mutants are labeled using the single letter code for each amino acid, followed by the residue number (in superscript) at which the substitution has been carried out.

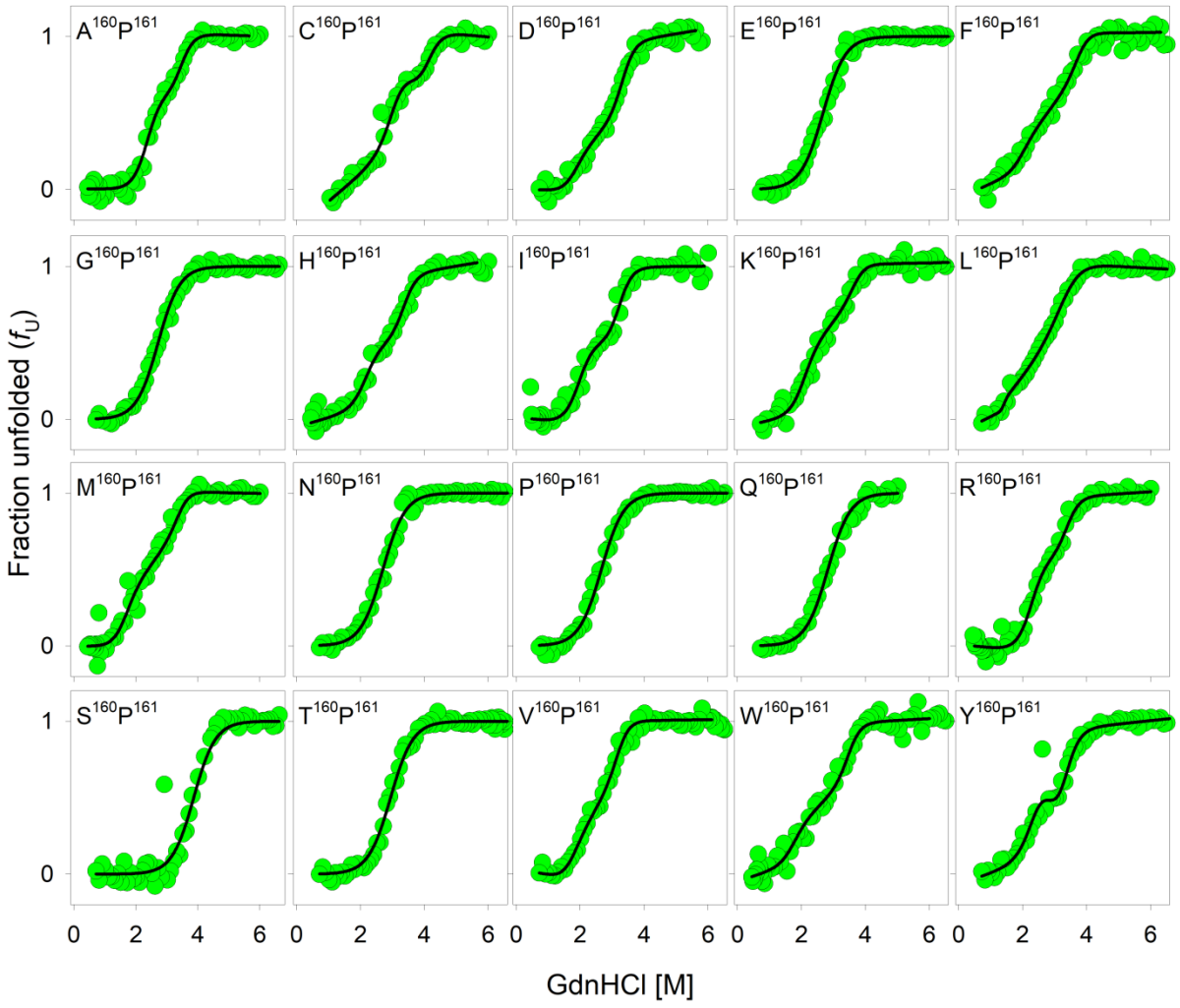

Figure S2. Equilibrium folding profiles of PagP-X^{160}P^{161} library. Unfolded protein fractions calculated from the change in tryptophan fluorescence emission intensity at the $\lambda_{em\text{-}max}$ of 344 nm are plotted against denaturant concentration for all mutants from the PagP-X^{160}P^{161} library. Data points are globally fitted either to the two-state equation[1] (for penultimate residues E, G, N, P, Q, S, and T at position 160) or three-state equation[2] (for all other residues at position 160) to derive the thermodynamic parameters. Folding profiles are represented as green symbols and fits are shown as black solid lines. Mutants are named with single-letter codes for residues present at the terminal two positions along with the residue number in superscript.

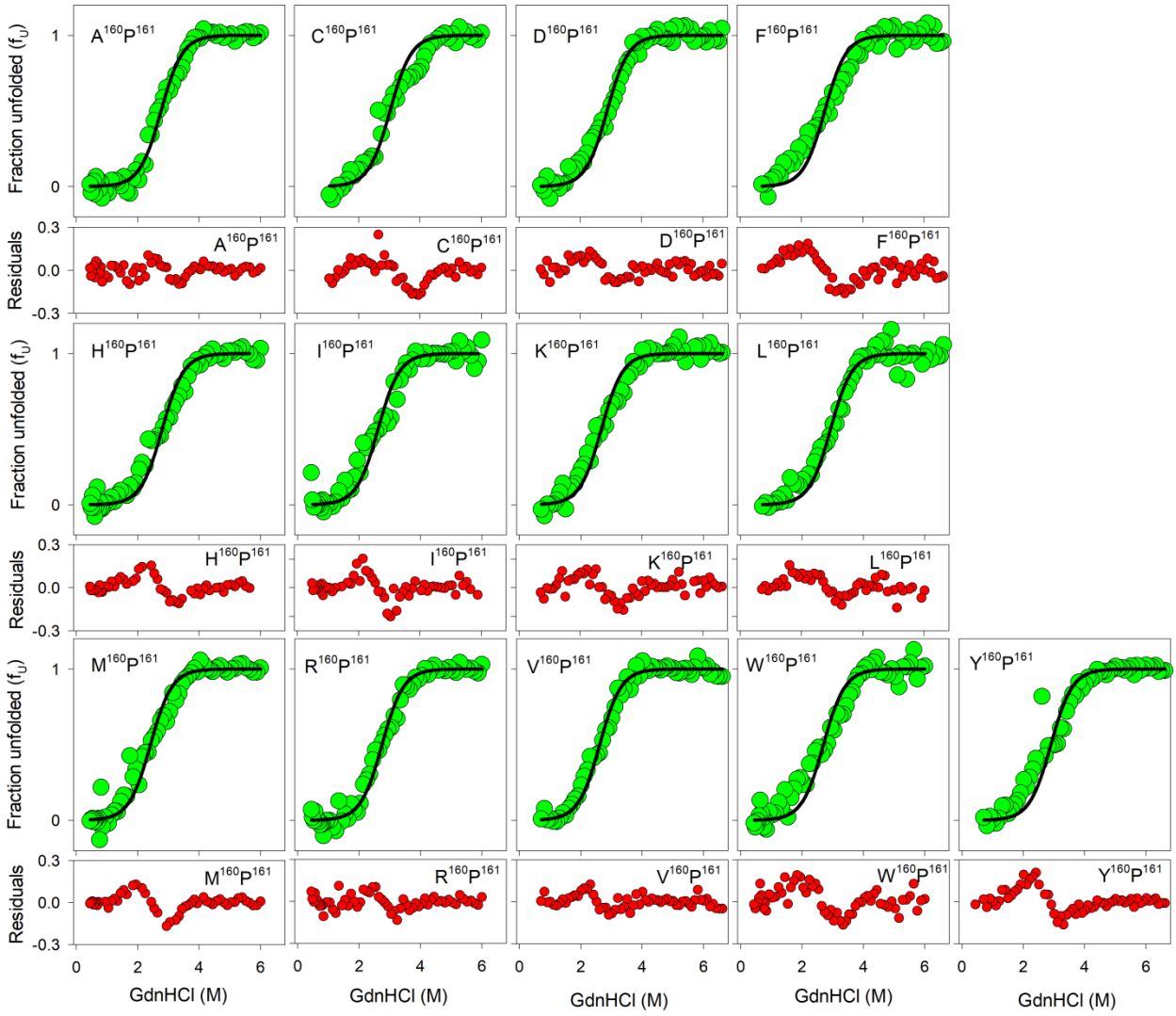

Figure S3. Equilibrium folding profiles for the PagP-$X^{160}P^{161}$ library. Unfolded protein fractions calculated from the change in tryptophan fluorescence emission intensity at the $\lambda_{em\text{-}max}$ of 344 nm for the folded protein are plotted against the respective denaturant concentrations for the three-state mutants of the PagP-$X^{160}P^{161}$ library. Data points are globally fitted to the two-state equation[1] using a global m value of 1.69 ± 0.03 kcal mol^{-1} M^{-1} to derive the thermodynamic parameters. Folding profiles are represented as green symbols and fits are shown as black solid lines. Residuals for the corresponding fits are shown as red scatter plots below each panel. Mutants are named with single-letter codes for residues present at the terminal two positions along with the residue number in superscript.

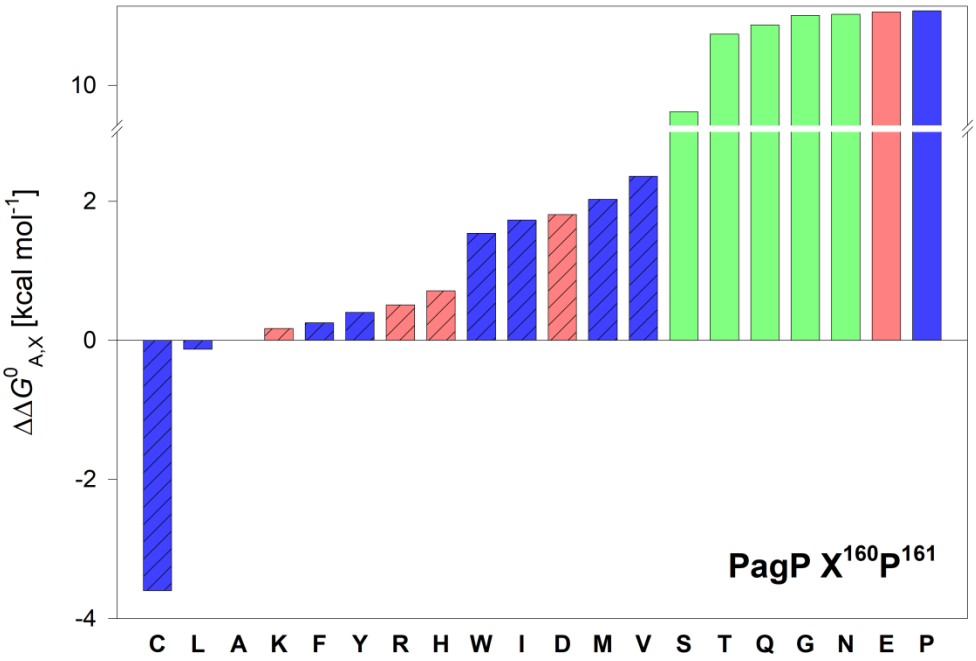

Figure S4. Normalized folding free energy for substitutions at the penultimate position of PagP-X^{160}P^{161} library. Equilibrium folding free energy measured for all 20 amino acids at the protein-facing hydrophilic interface (residue 160), normalized with respect to alanine. The energetic cost of partitioning of each residue at position 160 ($\Delta\Delta G^0_{A,X}$) showed a heterogeneous distribution of polar, hydrophobic, and charged residues. The color code and histogram representation are retained from Fig. 1D of the main text (blue, hydrophobic; red, hydrophilic; green, polar). Here, we found a skewed polarity scale, wherein hydrophobic residues (such as Leu and Phe) as well as charged residues (such as Lys and Arg) were favored over residues with small polar side chains (such as Ser and Thr).

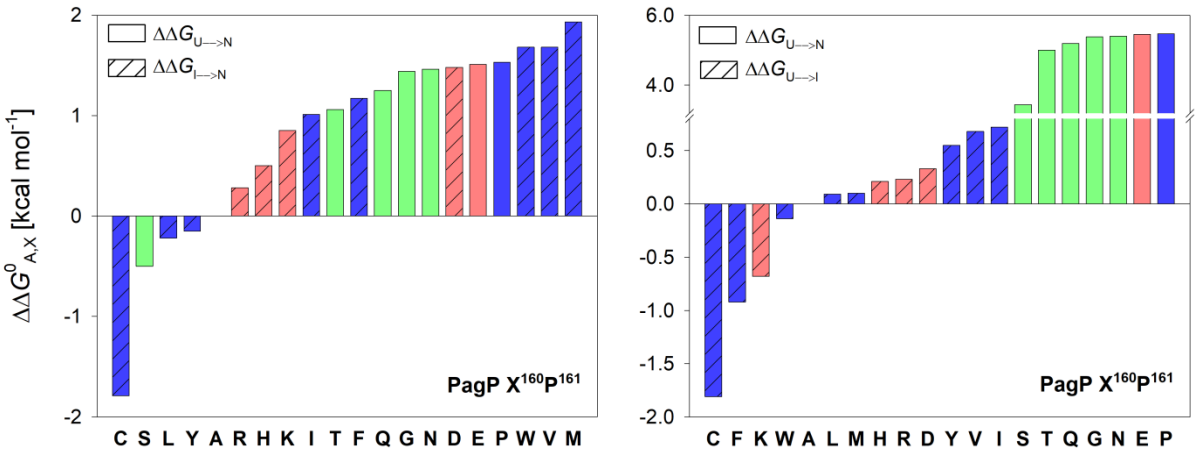

Figure S5. Normalized folding free energy at the penultimate position of PagP-$X^{160}P^{161}$ library. Histograms presenting the total change in folding free energy $\Delta\Delta G^0_{U\rightarrow N}$ for the PagP-$X^{160}P^{161}$ mutants exhibiting three-state folding profiles into $\Delta\Delta G^0_{I\rightarrow N}$ (left panel) and $\Delta\Delta G^0_{U\rightarrow I}$ (right panel), presented along with $\Delta\Delta G^0_{U\rightarrow N}$ for the mutants with two-state folding profiles. We find that hydrophobic and hydrophilic residues are dispersed across the hydrophobicity scale. Values from the three-state profiles are shown as a patterned fill in the histogram. The color code is retained from Fig. S4.

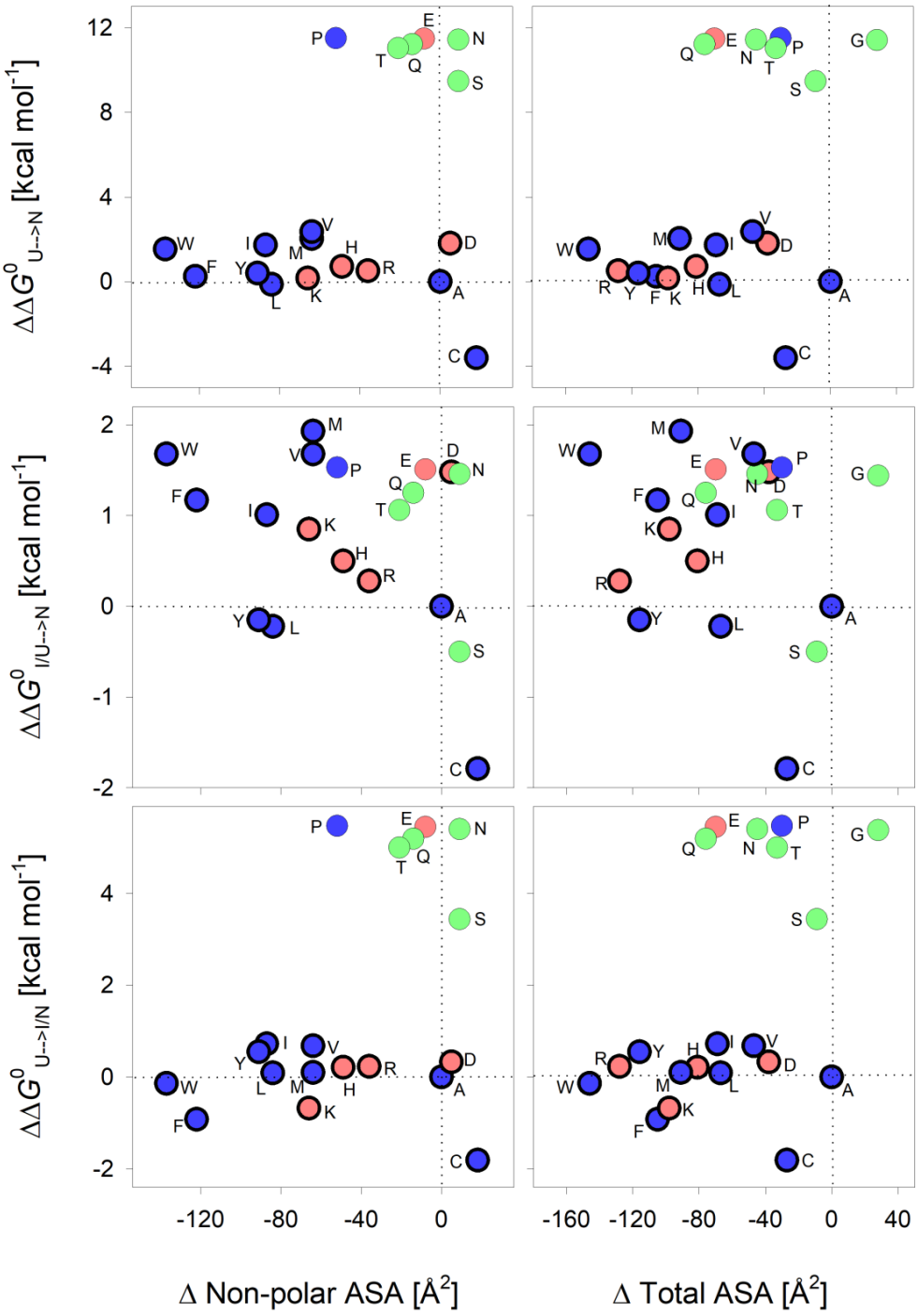

Figure S6. Correlation plots between $\Delta\Delta G^0$ and ASA change for the PagP-X^{160}P^{161} library. Correlation plots generated by mapping the total change in folding free energy $\Delta\Delta G^0_{U\rightarrow N}$ (upper panels) for the PagP-X^{160}P^{161} mutants against the change in per residue accessible surface area (ASA). The correlation plots are also generated by segregating the free energy of variants exhibiting three-state folding profiles into $\Delta\Delta G^0_{I\rightarrow N}$ (middle panels) and $\Delta\Delta G^0_{U\rightarrow I}$ (lower panels), presented along with $\Delta\Delta G^0_{U\rightarrow N}$ for the mutants with two-state folding profiles. For

purposes of correlation, we employed two empirical parameters describing the change in ASA – 1) the change in non-polar ASA per residue (left panels) and 2) the change in total ASA – both derived from previously reported calculations.[3] Variants displaying three-state profiles are shown as symbols with thicker edges. The color code has been retained from Fig. S4.

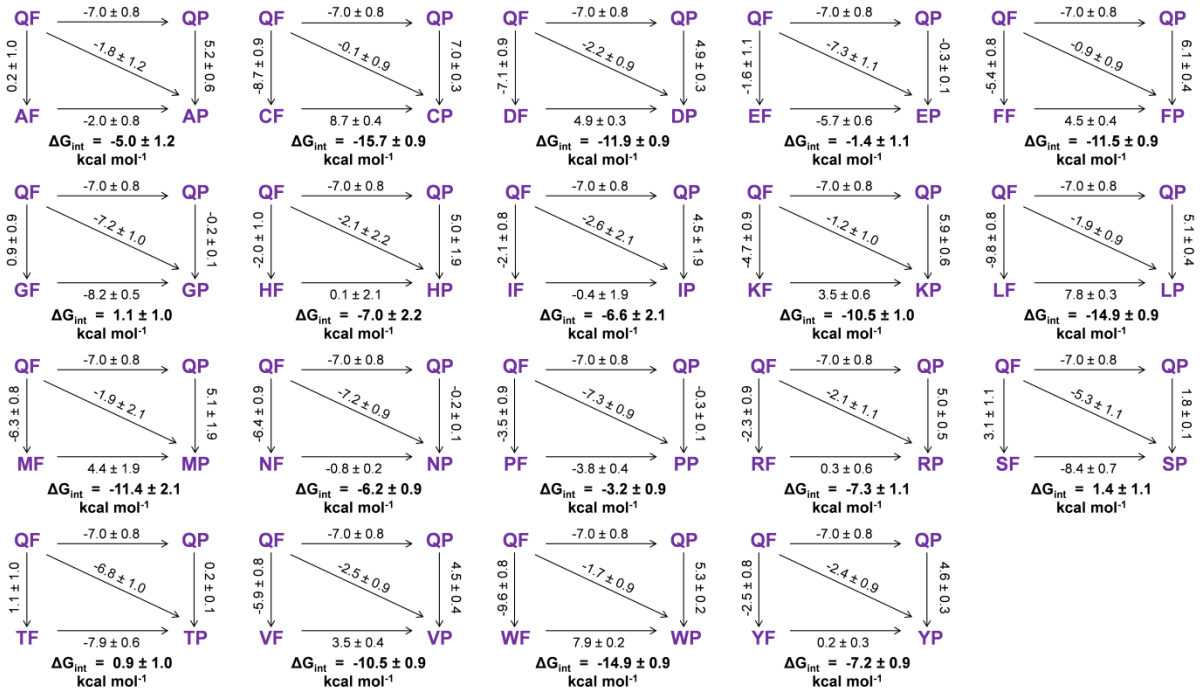

Figure S7. Double mutant cycles for estimating the interaction energy between the terminal and penultimate residue side chains in PagP. Folding free energy values obtained from the equilibrium titrations were used to carry out the double mutant cycle analysis to obtain the interaction energy (ΔG_{int}) as shown in Fig. 3 of the main text. For the PagP-$X^{160}P^{161}$ mutants exhibiting three-state folding profiles, we used the free energy value $\Delta G^0_{U\rightarrow I}$, representing the transition from the unfolded state (U) to the intermediate state (I). Residues at positions 160 and 161, respectively, are presented by their single-letter codes. The ΔG^0 values and interaction energies are reported in kcal mol^{-1}. Errors in some cases are omitted because reliable errors could not be derived for the mutants describing a three-state folding transitions.

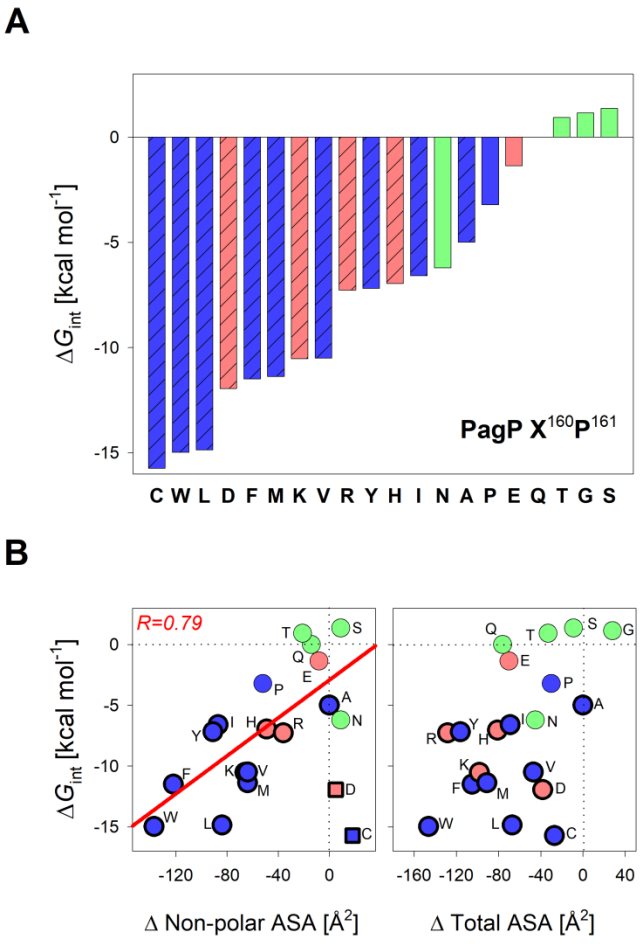

Figure S8. Correlation plot between the interaction energies derived for the PagP-X^{160}P^{161} mutants with the change in non-polar ASA per residue. (A) The interaction energy (ΔG_{int}) between the penultimate (X^{160}) and terminal (F^{161}) residues was computed for all 20 residue variants and are presented in decreasing order of ΔG_{int}. The color codes are retained from Fig. S4. Interaction energy values of mutants showing three-state profiles are shown as a patterned fill in the histogram. (B) Correlation between interaction energies (ΔG_{int}) and empirical parameters describing the change in ASA are shown as scatter plots. The ASA parameters are derived from previously reported calculations.[3] Variants with three-state folding profiles, for which the $\Delta G^0_{U\rightarrow I}$ has been used to compute the interaction energy, are shown as symbols with thicker edges. We find a strong correlation of the interaction energies with the change in non-polar ASA. In the left panel, a linear fit to the correlation is shown as a solid red line (R = 0.79). Points excluded from the fit are shown as square symbols. Residues are represented by their single-letter codes.

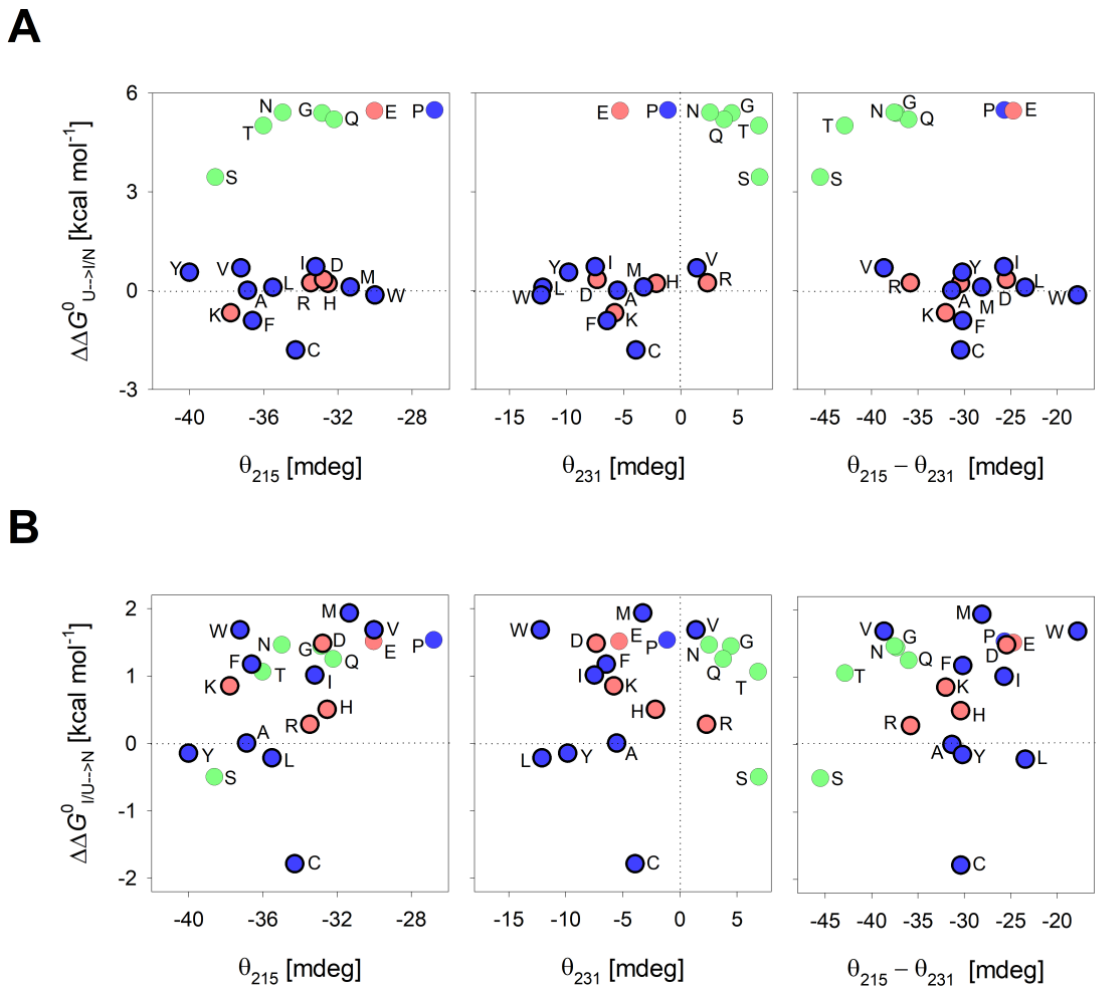

Figure S9. Correlation plots of $\Delta\Delta G^0$ and structural content for the PagP-X^{160}P^{161} library. We mapped the correlation of the secondary (θ_{215}, left panels) and tertiary (θ_{231}, middle panels) structural content with the folding free energy by segregating the total change in folding free energy $\Delta\Delta G^0_{U\rightarrow N}$ for the PagP-X^{160}P^{161} mutants exhibiting three-state folding profiles into (A) $\Delta\Delta G^0_{U\rightarrow I}$ and (B) $\Delta\Delta G^0_{I\rightarrow N}$, presented along with $\Delta\Delta G^0_{U\rightarrow N}$ for the mutants with two-state folding profiles. We further computed a parameter describing the difference in ellipticity between 215 nm and 231 nm ($\theta_{215} - \theta_{231}$, right panels in both A and B) to account for the ellipticity contribution from the tertiary exciton interaction to the negative maximum at 215 nm.[4] Variants displaying three-state profiles are shown as symbols with thicker edges. The color code has been retained from Fig. S4.

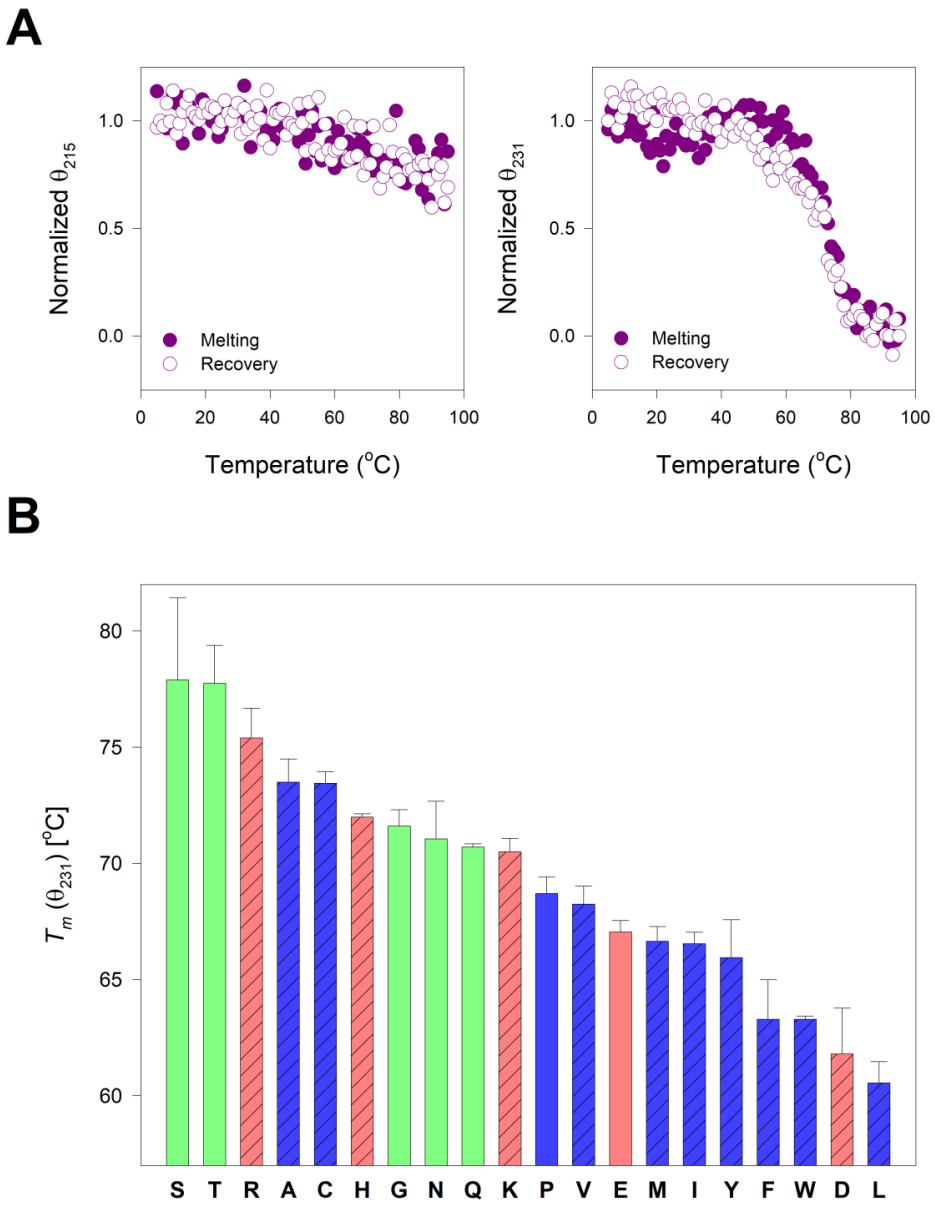

Figure S10. Effect of thermal denaturation on structural content of the PagP-X^{160}P^{161} library. (A) Representative unfolding (filled symbols) and refolding (open symbols) profiles recorded in response to thermal denaturation of PagP-Q^{160}P^{161} using spectropolarimetry (far-UV CD), by monitoring the process at 215 nm (θ_{215}, left panel) for β-sheet content and at 231 nm (θ_{231}, right panel) for changes in the exciton contribution. We find a completely reversible unfolding process for PagP, with ~30−40% loss in the secondary structure of the barrel (left panel), whereas the tertiary interaction shows a sigmoidal two-state reversible unfolding behavior in response to temperature (right panel). Only the θ_{231} data could be analyzed to derive the mid-point of thermal denaturation (T_m). (B) Comparison of T_m values derived for the CD thermal denaturation curves at 231 nm for the unfolding profiles of the PagP-X^{160}P^{161} library.

The mutants are named based on the residue present at the penultimate position (residue 160). Variants displaying three-state profiles in equilibrium folding are shown as a patterned fill in the histogram. The color code has been retained from Fig. S4. We find that hydrophilic residues demonstrate significantly higher $T_{m\text{-}231}$ (θ_{231}) values than hydrophobic residues. Errors represent the standard deviation calculated from two independent experiments.

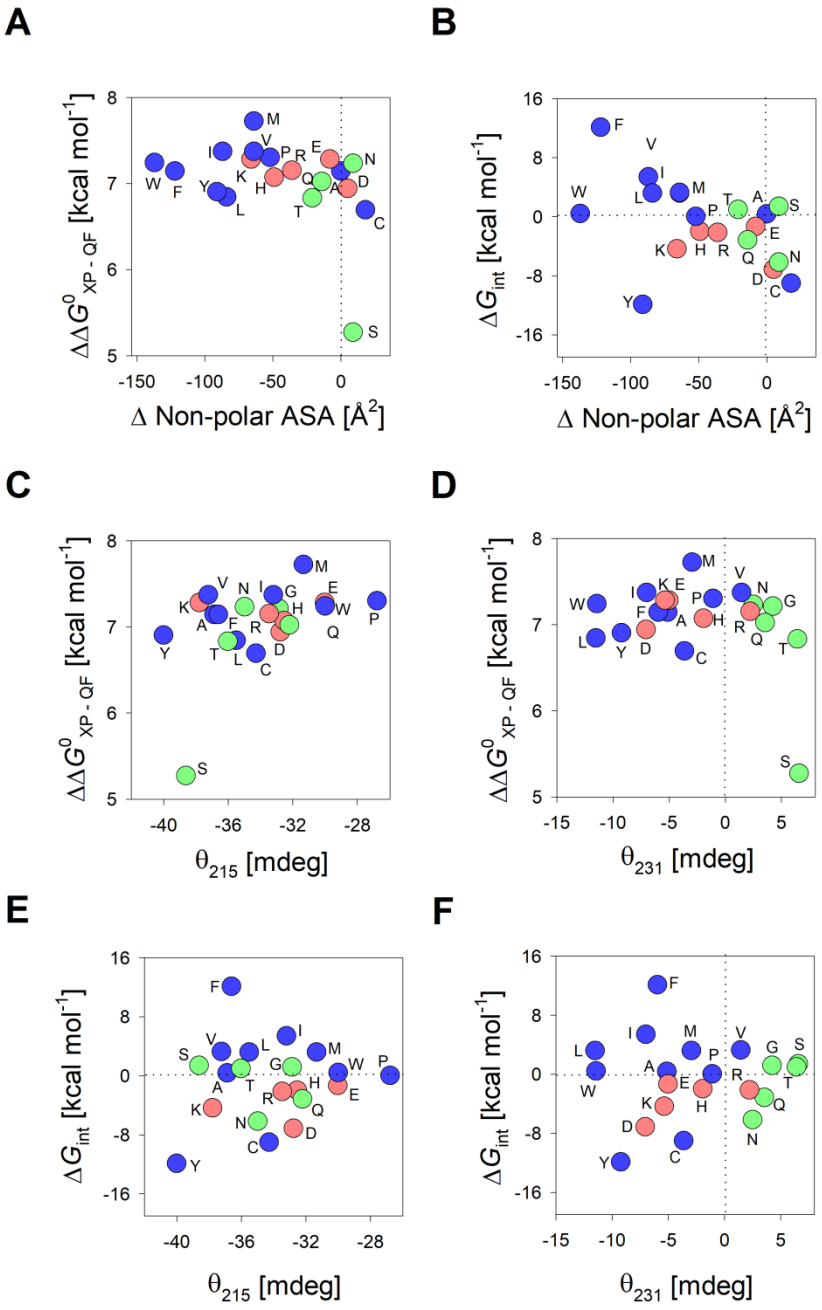

Figure S11. Correlation plots derived from comparison of thermodynamic parameters derived using two-state analysis of the PagP-X^{160}P^{161} library. Scatter plots correlating the parameters describing the non-polar ASA change with (A) the normalized free energy ($\Delta\Delta G^0_{XP\text{-}QF}$) and (B) the interaction energy (ΔG^0_{int}) derived for the library of mutants. Correlation plots for the (C) secondary structure content (θ_{215}) and (D) tertiary structure content (θ_{231}) with the change in free energy w.r.t. wild-type PagP ($\Delta\Delta G^0_{XP\text{-}QF}$) for all of the mutants. Correlation plots have also been generated for the (E) secondary structure content (θ_{215}) and (F) tertiary structure content (θ_{231}) with the interaction energy value (ΔG^0_{int}) for all of the mutants of the PagP-X^{160}P^{161} library. Scatter plots are colored based on the side chain properties as blue

(hydrophobic), red (hydrophilic), and green (polar). The color code has been retained from Fig. S4.

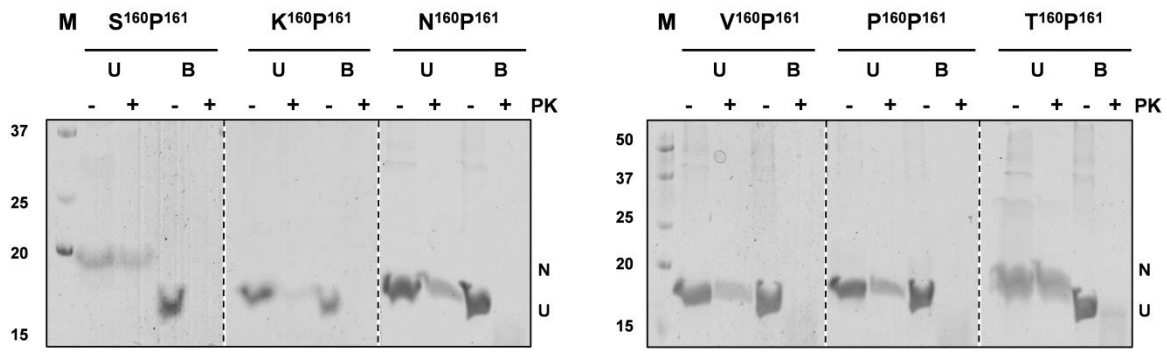

Figure S12. Electrophoretic mobility shift analysis and protease protection assay. Gel mobility shift on cold SDS-PAGE gels, and protection against proteolysis by proteinase K (PK) of representative mutants from the PagP-$X^{160}P^{161}$ library, was together used as evidence for the folded state of PagP variants. Samples folded into DPC micelles were categorized into unboiled (U) and boiled (B) based on whether they were subjected to a 3-min heat denaturation at 100 °C, prior to analysis on SDS-PAGE. Well-folded (native, N) and unfolded (U) proteins differ in their electrophoretic mobilities, with the folded PagP showing retarded mobility and resistance to PK digestion. The retarded gel mobility is due to the structural compaction achieved when the β-barrel scaffold is formed. Several mutants deviated from the typical retarded mobility demonstrated by wild-type PagP[2, 5] and show mobility resembling the unfolded protein, despite being folded in DPC micelles. These mutants showed varying levels of resistance to proteolysis by PK. The conspicuous absence of retarded gel mobility and susceptibility to proteolysis together indicate that, although structured, these mutants do not adopt the structurally compact β-barrel that is characteristic of PagP. Mutants are labeled using the single letter code for each amino acid, followed by the residue number (in superscript) at which the substitution has been carried out.

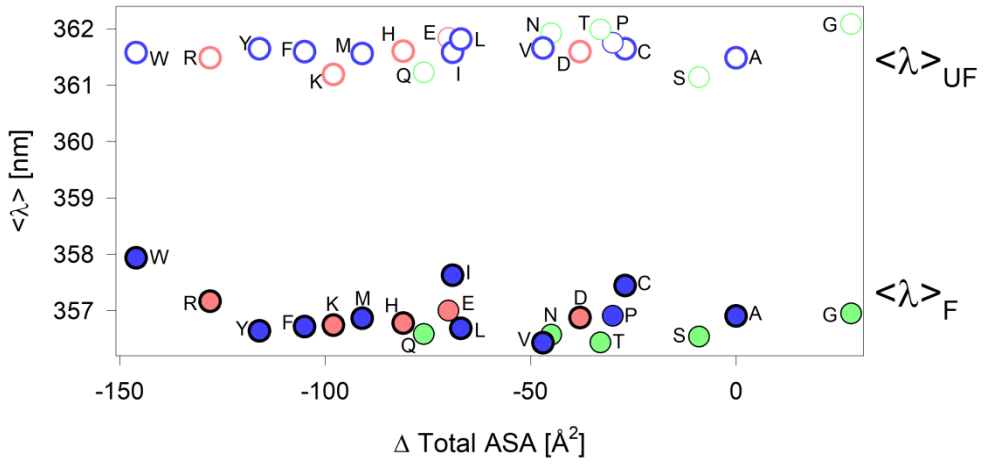

Figure S13. Correlation plot of Trp fluorescence for PagP-X^{160}P^{161} with the change in total ASA. The correlation plot compares the average wavelength[6] of the folded states ($\langle\lambda\rangle_F$, filled symbols) and average wavelength of the unfolded states ($\langle\lambda\rangle_{UF}$, hollow symbols) along the *y*-axis for all the mutants from the PagP-X^{160}P^{161} series with the ASA change per residue derived from previously reported calculations[3] (shown along the *x*-axis). All the residue variants exhibit similar average wavelength values with the $\langle\lambda\rangle_F$ averaging ~356.9 nm and the $\langle\lambda\rangle_{UF}$ averaging ~361.6 nm. This is a strong indicator that our fluorescence measurements capture the transition from the native state to the completely unfolded state. It is important to note here that the $\langle\lambda\rangle$ value is a reflection of the local environment of all 12 tryptophans. While it can be argued that Trp fluorescence is not necessarily a direct indicator that the mutants have attained the native state, the 12 Trp residues are not only spread across the sequence and the β-barrel scaffold, the data for all the mutants are similar (irrespective of their folding pathway and thermal stability), which together supports our conclusion that all PagP variants in this library are indeed folded and transition to the fully unfolded state upon chemical denaturation. Variants displaying three-state profiles are shown as symbols with thicker edges. The color code has been retained from Fig. S4.

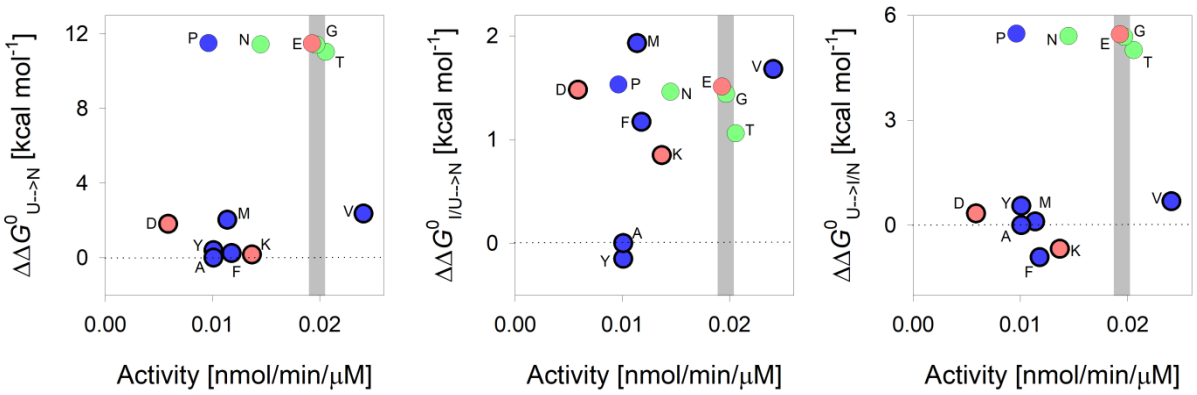

Figure S14. Correlation plots between the catalytic activity and thermodynamic stability for PagP-X^{160}P^{161} library. We derived correlation plots by mapping the catalytic activity values for mutants from the PagP-X^{160}P^{161} series with the corresponding change in the equilibrium folding free energy. We generated the plots by segregating the total change in folding free energy $\Delta\Delta G^0_{U\rightarrow N}$ (left panel) for the PagP-X^{160}P^{161} mutants exhibiting three-state folding profiles into $\Delta\Delta G^0_{I\rightarrow N}$ (middle panel) and $\Delta\Delta G^0_{U\rightarrow I}$ (right panel) and presenting them along with $\Delta\Delta G^0_{U\rightarrow N}$ for the mutants with two-state folding profiles. Variants displaying three-state profiles are shown as symbols with thicker edges. The color code has been retained from Fig. S4.

SI REFERENCES

1. Santoro, M. M., and Bolen, D. W. (1988) Unfolding free energy changes determined by the linear extrapolation method. 1. Unfolding of phenylmethanesulfonyl alpha-chymotrypsin using different denaturants. *Biochemistry 27*, 8063-8068.
2. Iyer, B. R., Zadafiya, P., Vetal, P. V., and Mahalakshmi, R. (2017) Energetics of side-chain partitioning of beta-signal residues in unassisted folding of a transmembrane beta-barrel protein. *J. Biol. Chem. 292*, 12351-12365.
3. Miller, S., Janin, J., Lesk, A. M., and Chothia, C. (1987) Interior and surface of monomeric proteins. *J. Mol. Biol. 196*, 641-656.
4. Khan, M. A., Neale, C., Michaux, C., Pomes, R., Prive, G. G., Woody, R. W., and Bishop, R. E. (2007) Gauging a hydrocarbon ruler by an intrinsic exciton probe. *Biochemistry 46*, 4565-4579.
5. Iyer, B. R., and Mahalakshmi, R. (2015) Residue-Dependent Thermodynamic Cost and Barrel Plasticity Balances Activity in the PhoPQ-Activated Enzyme PagP of Salmonella typhimurium. *Biochemistry 54*, 5712-5722.
6. Moon, C. P., and Fleming, K. G. (2011) Using tryptophan fluorescence to measure the stability of membrane proteins folded in liposomes. *Methods Enzymol. 492*, 189-211.